The Star Formation Newsletter

A community newsletter on Star and Planet Formation research

No. 343 — 25 July 2021
Editor: João Alves www.starformation.news

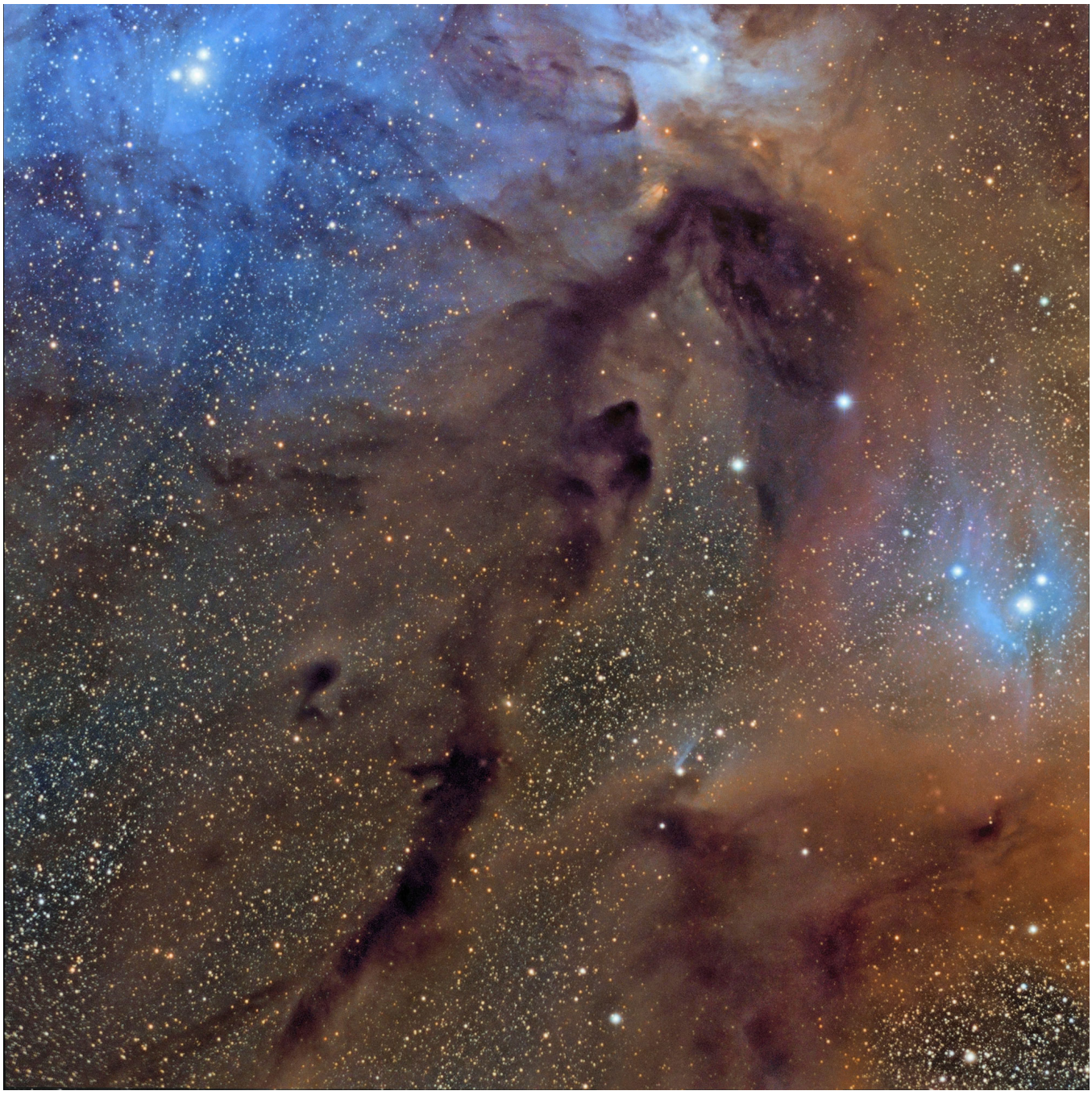

Links to sections

Interviews	Reviews	Perspective	Favorite objects	Archive
Meetings	Jobs	New PhDs	Announcements	Books

Cover image caption

Amazing Ophiuchus, a Summer favorite. The ρ Oph cluster is shown at the upper left (the three bright stars mark the cluster center). L1688, the dark clump towards the upper right, contains the closest embedded cluster of YSOs. Many famous and well-studied young sources, that played a fundamental role in early star formation studies, are hidden in this optical image. The L1689 cloud lies to the lower right, below L1688, while L1709 and Oph D are seen towards the center of the image. Credit: Leonardo Ciuffolotti, Matteo Collina, Riccardo De Benedictis, Giuseppe Donatiello, Rolando Ligustri.

Note from the Editor

The Star Formation Newsletter is now on the web at **www.starformation.news**. This PDF file contains the monthly Abstracts and links to the different Newsletter sections. Red text in this PDF is a url link. Submitting an abstract to the SFN is as simple as entering the arXiv ID (e.g., 2006.10139) in a web form on the SFN web site. **Do not remove the LaTeX formatting when submitting to the arXiv**. If you do, your abstract will not look great either at the arXiv (which uses MathJax to convert LaTeX math symbols to the web) or the SFN.

Abstracts

1. ## Multi-scale Dust Polarization and Spiral-like Stokes-I Residual in the Class I Protostellar System TMC-1A

Yusuke Aso, Woojin Kwon, Naomi Hirano, Tao-Chung Ching, Shih-Ping Lai, Zhi-Yun Li, Ramprasad Rao

We have observed the Class I protostar TMC-1A in the Taurus molecular cloud using the Submillimeter Array (SMA) and the Atacama Large Millimeter/submillimeter Array (ALMA) in the linearly polarized 1.3 mm continuum emission at angular resolutions of 3" and 0.3", respectively. The ALMA observations also include CO, 13CO, and C18O J=2-1 spectral lines. The SMA observations trace magnetic fields on the 1000-au scale, the directions of which are neither parallel nor perpendicular to the outflow direction. Applying the Davis-Chandrasekhar-Fermi method to the SMA polarization angle dispersion, we estimate a field strength in the TMC-1A envelope of 1-5 mG. It is consistent with the field strength needed to reduce the radial infall velocity to the observed value, which is substantially less than the local free-fall velocity. The ALMA polarization observations consist of two distinct components – a central component and a north/south component. The central component shows polarization directions in the disk minor axis to be azimuthal, suggesting dust self-scattering in the TMC-1A disk. The north/south component is located along the outflow axis and the polarization directions are aligned with the outflow direction. We discuss possible origins of this polarization structure, including grain alignment by a toroidal magnetic field and mechanical alignment by the gaseous outflow. In addition, we discover a spiral-like residual in the total intensity (Stokes I) for the first time. The C18O emission suggests that material in the spiral-like structure is infalling at a speed that is 20the local Keplerian speed.

2. ## PV Cep and V350 Cep: stars on the way between FUors AND EXors

H. R. Andreasyan, T. Yu. Magakian, T. A. Movsessian, A. V. Moiseev

Based on new observations during 2015-2020 and published data, the unusual eruptive variables PV Cep and V350 Cep are examined. It is shown that PV Cep underwent a regular outburst followed by a drop in brightness that lasted overall from 2011 to 2019 and is still in a deep minimum. The outburst was accompanied by substantial changes in the intensity and profiles of a number of lines, including Ha, [SII], and [OI]. The forbidden lines generally have negative radial velocities and can be divided into four components, with variable velocities and relative intensities. V350 Cep essentially is at a maximum brightness level over the entire time and its spectrum is practically unaltered. The available data suggest that the pronounced P Cyg profile of the Ha line in the spectrum of V350 Cep appeared several years after the luminosity rise, in 1986. The luminosities of the stars

in the current state are estimated to be 20 L(sun) and 3.3 L(sun), respectively. It is concluded that both stars may represent a so-called intermediate objects between the FUor and EXor classes.

3. GIARPS High-resolution Observations of T Tauri stars (GHOsT). III. A pilot study of stellar and accretion properties

J. M. Alcalá, M. Gangi, K. Biazzo, S. Antoniucci, A. Frasca, T. Giannini, U. Munari, B. Nisini, A. Harutyunyan, C. F. Manara, F. Vitali

The mass-accretion rate, Macc, is a crucial parameter for the study of the evolution of accretion disks around young low-mass stellar objects (YSOs) and for planet formation studies. The Taurus star forming region (SFR) is rich in pre-main sequence (PMS) stars, most of them of the T Tauri class. A variety of methodologies have been used in the past to measure mass accretion in samples of YSOs in Taurus, but despite being a general benchmark for star formation studies, a comprehensive and systematic analysis of the Taurus T Tauri population, where the stellar and accretion properties are derived homogeneously and simultaneously, is still missing. As part of the GIARPS High-resolution Observations of T Tauri stars (GHOsT) project, here we present a pilot study of the stellar and accretion properties of seven YSOs in Taurus using the spectrograph GIARPS at the Telescopio Nazionale Galileo (TNG). Contemporaneous low-resolution spectroscopic and photometric ancillary observations allow us to perform an accurate flux calibration of the high-resolution spectra. The simultaneity of the high-resolution, wide-band spectroscopic observations, from the optical to the near-infrared (NIR), the veiling measurements in such wide spectral range, and many well-calibrated emission line diagnostics allows us to derive the stellar and accretion properties of the seven YSOs in a homogeneous and self-consistent way. The procedures and methodologies presented here will be adopted in future works for the analysis of the complete GHOsT data set. We discuss the accretion properties of the seven YSOs in comparison with the 90% complete sample of YSOs in the Lupus SFR and investigate possibilities for the origin of the continuum excess emission in the NIR.

4. Evolution of the angular momentum during gravitational fragmentation of molecular clouds

G. Arroyo-Chávez, E. Vázquez-Semadeni

We investigate the origin of the observed scaling $j \sim R^{3/2}$ between the specific angular momentum j and the radius R of molecular clouds (MCs) and their their substructures, and of the observed near independence of β, the ratio of rotational to gravitational energy, from R. To this end, we measure the angular momentum (AM) of sets of particles in an SPH simulation of the formation, collapse and fragmentation of giant MCs. The sets of SPH particles are defined either as "clumps" (connected particle sets), or as lagrangian sets that conform a connected clump only at a certain time $tdef$. We find that: *i)* Clumps evolve along the observed jR relation at all times, *ii)* Lagrangian particle sets evolve along the observed relation when the volume containing them also contains a large number of other "intruder" particles. Otherwise, they evolve with $j \sim$ cst. *iii)* Tracking lagrangian sets to the future, we find that a subset of the SPH particles participates in the collapse, while another disperses away. *iv)* Noting that, under AM conservation, β increases during contraction, we suggest that its near independence of radius may arise from the competition between this increase and an increase in the AM exchange rate at higher rotational energy density gradient. *v)* We suggest that, if MCs are globally dominated by gravity, the observed jR relation arises because the observational selection of its dense structures amounts to selecting the fragments that have lost AM via Reynolds stresses from their neighbors.

5. Classification of Filament Formation Mechanisms in Magnetized Molecular Clouds

Daisei Abe, Tsuyoshi Inoue, Shu-ichiro Inutsuka, Tomoaki Matsumoto

Recent observations of molecular clouds show that dense filaments are the sites of present-day star formation. Thus, it is necessary to understand the filament formation process because these filaments provide the initial condition for star formation. Theoretical research suggests that shock waves in molecular clouds trigger filament formation. Since several different mechanisms have been proposed for filament formation, the formation mechanism of the observed star-forming filaments requires clarification. In the present study, we perform a series of isothermal magnetohydrodynamics simulations of filament formation. We focus on the influences of shock velocity and turbulence on the formation mechanism and identified three different mechanisms for the filament formation. The results indicate that when the shock is fast, at shock velocity $v_{sh} = 7$ km/s, the gas flows driven by the curved shock wave create filaments irrespective of the presence of turbulence and self-gravity. However, at a slow shock velocity $v_{sh} = 2.5$ km/s, the compressive flow component involved in the initial turbulence induces filament formation. When both the shock velocities and turbulence are low, the self-gravity in the shock-compressed sheet becomes important for filament formation. Moreover, we analyzed the line-mass distribution of the filaments and showed that strong shock waves can naturally

create high-line-mass filaments such as those observed in the massive star-forming regions in a short time. We conclude that the dominant filament formation mode changes with the velocity of the shock wave triggering the filament formation.

6. Detection of coherent low-frequency radio bursts from weak-line TTauri stars

A. Feeney-Johansson, S. J. D. Purser, T. P. Ray, A. A. Vidotto, J. Eislöffel, J. R. Callingham, T. W. Shimwell, H. K. Vedantham, G. Hallinan, C. Tasse

In recent years, thanks to new facilities such as LOFAR capable of sensitive observations, much work has been done on the detection of stellar radio emission at low frequencies. Such emission has commonly been shown to be coherent emission, generally attributed to electron-cyclotron maser emission, and has usually been detected from main-sequence M dwarfs. Here we report the first detection of coherent emission at low frequencies from T Tauri stars, which are known to be associated with high levels of stellar activity. Using LOFAR, we have detected several bright radio bursts at 150 MHz from two weak-line T Tauri stars: KPNO-Tau 14 and LkCa 4. All of the bursts have high brightness temperatures ($10^{13} - 10^{14}$ K) and high circular polarization fractions (60 - 90 %), indicating that they must be due to a coherent emission mechanism. This could be either plasma emission or electron-cyclotron maser (ECM) emission. Due to the exceptionally high brightness temperatures seen in at least one of the bursts ($\geq 10^{14}$ K), and the high circular polarization levels, it seems unlikely that plasma emission could be the source and so ECM is favoured as the most likely emission mechanism. Assuming this is the case, the required magnetic field in the emission regions would be 40 - 70 G. We determine that the most likely method of generating ECM emission is plasma co-rotation breakdown in the stellar magnetosphere. There remains the possibility, however, it could be due to an interaction with an orbiting exoplanet.

7. The Transition from Diffuse Molecular Gas to Molecular Cloud Material in Taurus

S. R. Federman, Johnathan S. Rice, A. M. Ritchey, Hwihyun Kim, John H. Lacy, Paul F. Goldsmith, Nicolas Flagey, Gregory N. Mace, David L. Lambert

We study four lines of sight that probe the transition from diffuse molecular gas to molecular cloud material in Taurus. Measurements of atomic and molecular absorption are used to infer the distribution of species and the physical conditions toward stars behind the Taurus Molecular Cloud (TMC). New high-resolution spectra at visible and near infrared wavelengths of interstellar Ca II, Ca I, K I, CH, CH^+, C2, CN, and CO toward HD28975 and HD29647 are combined with data at visible wavelengths and published CO results from ultraviolet measurements for HD27778 and HD30122. Gas densities and temperatures are inferred from C2, CN, and CO excitation and CN chemistry. Our results for HD29647 are noteworthy because the CO column density is 10^{18} cm^{-2} while C2 and CO excitation reveals a temperature of 10 K and density about 1000 cm^{-3}, more like conditions found in dark molecular clouds. Similar results arise from our chemical analysis for CN through reactions involving observations of CH, C2, and NH. Enhanced potassium depletion and a reduced CH/H2 column density ratio also suggest the presence of a dark cloud. The directions toward HD27778 and HD30122 probe molecule-rich diffuse clouds, which can be considered CO-dark gas, while the sight line toward HD28975 represents an intermediate case. Maps of dust temperature help refine the description of the material along the four sight lines and provide an estimate of the distance between HD29647 and a clump in the TMC. An Appendix provides results for the direction toward HD26571; this star also probes diffuse molecular gas.

8. SIRIUS Project. III. Star-by-star simulations of star cluster formation using a direct N-body integrator with stellar feedback

Michiko S. Fujii, Takayuki R. Saitoh, Yutaka Hirai, Long Wang

One of the computational challenges of cluster formation simulations is resolving individual stars and simulating massive clusters with masses of more than $10^4 M_\odot$ without gravitational softening. Combining direct N-body code with smoothed-particle hydrodynamics (SPH) code, we have developed a new code, ASURA+BRIDGE, in which we can integrate stellar particles without softening. We add a feedback model for HII regions into this code, in which thermal and momentum feedback is given within the Strömgren radius. We perform N-body/SPH simulations of star cluster formation. Without softening, a portion of massive stars are ejected from the forming clusters. As a result, the stellar feedback works outside the clusters. This enhances/suppresses the star formation in initially sub-virial/super-virial clouds. We find that the formed star clusters are denser than currently observed open clusters, but the mass–density relation is consistent with or even higher than that is estimated as an initial cluster density. We also find that some clusters have multiple peaks in their stellar age distribution as a consequence of their hierarchical formation.

9. X-ray Super-Flares From Pre-Main Sequence Stars: Flare Modeling

Konstantin V. Getman, Eric D. Feigelson, Gordon P. Garmire

Getman et al. (2021) reports the discovery, energetics, frequencies, and effects on environs of > 1000 X-ray super-flares with X-ray energies $E_X \sim 10^{34} - 10^{38}$ erg from pre-main sequence (PMS) stars identified in the *Chandra* MYStIX and SFiNCs surveys. Here we perform detailed plasma evolution modeling of 55 bright MYStIX/SFiNCs super-flares from these events. They constitute a large sample of the most powerful stellar flares analyzed in a uniform fashion. They are compared with published X-ray super-flares from young stars in the Orion Nebula Cluster, older active stars, and the Sun. Several results emerge. First, the properties of PMS X-ray super-flares are independent of the presence or absence of protoplanetary disks inferred from infrared photometry, supporting the solar-type model of PMS flaring magnetic loops with both footpoints anchored in the stellar surface. Second, most PMS super-flares resemble solar long duration events (LDEs) that are associated with coronal mass ejections. Slow rise PMS super-flares are an interesting exception. Third, strong correlations of super-flare peak emission measure and plasma temperature with the stellar mass are similar to established correlations for the PMS X-ray emission composed of numerous smaller flares. Fourth, a new correlation of loop geometry is linked to stellar mass; more massive stars appear to have thicker flaring loops. Finally, the slope of a long-standing relationship between the X-ray luminosity and magnetic flux of various solar-stellar magnetic elements appears steeper in PMS super-flares than for solar events.

10. The Macroporosity of Rubble Pile Asteroid Ryugu and Implications for the Origin of Chondrules

William Herbst, James P. Greenwood, Teng Ee Yap

We use the known surface boulder-size distribution of the C-type rubble pile asteroid Ryugu (NEA 162173) to determine its macroporosity, assuming it is a homogeneous granular aggregate. We show that the volume-frequency distribution of its boulders, cobbles and pebbles, is well represented by a lognormal function with $\sigma = 2.4 \pm 0.1$ and $\mu = 0.2 \pm 0.05$. Application of linear-mixture packing theory yields a value for the macroporosity of $\phi = 0.14 \pm 0.04$. Given its low bulk density of 1.19 gm cm^{-3}, this implies an average density for Ryugu's rocks of 1.38 ± 0.07 gm cm^{-3} throughout its volume, consistent with a recent determination for surface boulders based on their thermal properties. This supports the spectrum-based argument that IDP's may be the best analog material available on Earth and suggests that high-density, well-lithified objects such as chondrules and chondrule-bearing chondrites may be rare on Ryugu. Implications of this result for the origin of chondrules, a long-standing problem in cosmochemistry, are discussed. We propose that chondrules and most chondrites formed together in rare lithification events, which occurred during the accretion of chondritic envelopes to large, differentiated planetesimals at a time when they were still hot from ^{26}Al decay.

11. Misaligned Circumstellar Disks and Orbital Motion of the Young Binary XZ Tau

Takanori Ichikawa, Miyu Kido, Daisuke Takaishi, Yoshito Shimajiri, Yusuke Tsukamoto, Shigehisa Takakuwa

We report our analyses of the multi-epoch (2015-2017) ALMA archival data of the Class II binary system XZ Tau at Bands 3, 4 and 6. The millimeter dust continuum images show compact, unresolved (r < 15 au) circumstellar disks (CSDs) around the individual binary stars; XZ Tau A and B, with a projected separation of 39 au. The 12CO (2-1) emission associated with those CSDs traces the Keplerian rotations, whose rotational axes are misaligned with each other (P.A. -5 deg for XZ Tau A and 130 deg for XZ Tau B). The similar systemic velocities of the two CSDs (VLSR 6.0 km s-1) suggest that the orbital plane of the binary stars is close to the plane of the sky. From the multi-epoch ALMA data, we have also identified the relative orbital motion of the binary. Along with the previous NIR data, we found that the elliptical orbit (e = 0.742+0.025-0.034, a = 0".172+0".002-0".003, and ω = -54.2+2.0-4.7 deg) is preferable to the circular orbit. Our results suggest that the two CSDs and the orbital plane of the XZ Tau system are all misaligned with each other, and possible mechanisms to produce such a configuration are discussed. Our analyses of the multi-epoch ALMA archival data demonstrate the feasibility of time-domain science with ALMA.

12. ALMA observations of doubly deuterated water: Inheritance of water from the prestellar environment

S. S. Jensen, J. K. Jørgensen, L. E. Kristensen, A. Coutens, E. F. van Dishoeck, K. Furuya, D. Harsono, M. V. Persson

Establishing the origin of the water D/H ratio in the Solar System is central to our understanding of the chemical trail of water during the star and planet formation process. Recent modeling suggests that comparisons of the D_2O/HDO and HDO/H_2O ratios are a powerful way to trace the chemical evolution of water and, in particular, determine whether the D/H ratio is inherited

from the molecular cloud or established locally. We seek to determine the D_2O column density and derive the D_2O/HDO ratios in the warm region toward the low-mass Class 0 sources B335 and L483. The results are compared with astrochemical models and previous observations to determine their implications for the chemical evolution of water. We present ALMA observations of the D_2O transition at 316.8 GHz toward B335 and L483 at <0.5" (< 100 au) resolution, probing the inner warm envelope gas. The column densities of D_2O, HDO, and $H_2^{18}O$ are determined by synthetic spectrum modeling and direct Gaussian fitting, under the assumption of a single excitation temperature and similar spatial extent for the three water isotopologs. D_2O is detected toward both sources in the inner warm envelope. The derived D_2O/HDO ratios is $(1.0 \pm 0.2) \times 10^{-2}$ for L483 and $(1.4 \pm 0.1) \times 10^{-2}$ for B335. The high D_2O/HDO ratios are a strong indication of chemical inheritance of water from the prestellar phase down to the inner warm envelope. This implies that the local cloud conditions in the prestellar phase, such as temperatures and timescales, determine the water chemistry at later stages and could provide a source of chemical differentiation in young systems. In addition, the observed D_2O/H_2O ratios support an observed dichotomy in the deuterium fractionation of water toward isolated and clustered protostars, namely, a higher D/H ratio toward isolated sources

13. A Deep Search for Five Molecules in the 49 Ceti Debris Disk

Jessica Klusmeyer, A. Meredith Hughes, Luca Matra, Kevin Flaherty, Agnes Kospal, Attila Moor, Aki Roberge, Karin Oberg, Aaron Boley, Jacob White, David Wilner, Peter Abraham

Surprisingly strong CO emission has been observed from more than a dozen debris disks around nearby main-sequence stars. The origin of this CO is unclear, in particular whether it is left over from the protoplanetary disk phase or is second-generation material released from collisions between icy bodies like debris dust. The primary unexplored avenue for distinguishing the origin of the material is understanding its molecular composition. Here we present a deep search for five molecules (CN, HCN, HCO+, SiO, and CH3OH) in the debris disk around 49 Ceti. We take advantage of the high sensitivity of the Atacama Large Millimeter/submillimeter Array (ALMA) at Band 7 to integrate for 3.2 hours at modest spatial (1") and spectral (0.8 km/s) resolution. Our search yields stringent upper limits on the flux of all surveyed molecular lines, which imply abundances relative to CO that are orders of magnitude lower than those observed in protoplanetary disks and Solar System comets, and also those predicted in outgassing models of second-generation material. However, if CI shielding is responsible for extending the lifetime of any CO produced in second-generation collisions, as proposed by Kral et al. (2018), then the line ratios do not reflect true ice phase chemical abundances, but rather imply that CO is shielded by its own photodissociation product, CI, but other molecules are rapidly photodissociated by the stellar and interstellar radiation field.

14. A high pitch angle structure in the Sagittarius Arm

M. A. Kuhn, R. A. Benjamin, C. Zucker, A. Krone-Martins, R. S. de Souza, A. Castro-Ginard, E. E. O. Ishida, M. S. Povich, L. A. Hillenbrand

Context: In spiral galaxies, star formation tends to trace features of the spiral pattern, including arms, spurs, feathers, and branches. However, in our own Milky Way, it has been challenging to connect individual star-forming regions to their larger Galactic environment owing to our perspective from within the disk. One feature in nearly all modern models of the Milky Way is the Sagittarius Arm, located inward of the Sun with a pitch angle of 12 deg. Aims: We map the 3D locations and velocities of star-forming regions in a segment of the Sagittarius Arm using young stellar objects (YSOs) from the Spitzer/IRAC Candidate YSO (SPICY) catalog to compare their distribution to models of the arm. Methods: Distances and velocities for these objects are derived from Gaia EDR3 astrometry and molecular line surveys. We infer parallaxes and proper motions for spatially clustered groups of YSOs and estimate their radial velocities from the velocities of spatially associated molecular clouds. Results: We identify 25 star-forming regions in the Galactic longitude range l 4.0-18.5 deg arranged in a narrow, 1 kpc long linear structure with a high pitch angle of $\psi = 56$ deg and a high aspect ratio of 7:1. This structure includes massive star-forming regions such as M8, M16, M17, and M20. The motions in the structure are remarkably coherent, with velocities in the direction of Galactic rotation of 240 ± 3 km/s (slightly higher than average) and slight drifts toward the Galactic center (-4.3 km/s) and in the negative Z direction (-2.9 km/s). The rotational shear experienced by the structure is 4.6 km/s/kpc. Conclusions: The observed 56 deg pitch angle is remarkably high for a segment of the Sagittarius Arm. We discuss possible interpretations of this feature as a substructure within the lower pitch angle Sagittarius Arm, as a spur, or as an isolated structure.

15. The density structure of supersonic self-gravitating turbulence

Shivan Khullar, Christoph Federrath, Mark R. Krumholz, Christopher D. Matzner

We conduct numerical experiments to determine the density probability distribution function (PDF) produced in supersonic, isothermal, self-gravitating turbulence of the sort that is ubiquitous in star-forming molecular clouds. Our experiments cover a

wide range of turbulent Mach number and virial parameter, allowing us for the first time to determine how the PDF responds as these parameters vary, and we introduce a new diagnostic, the dimensionless star formation efficiency versus density ($\epsilon_{\rm ff}(s)$) curve, which provides a sensitive diagnostic of the PDF shape and dynamics. We show that the PDF follows a universal functional form consisting of a log-normal at low density with two distinct power law tails at higher density; the first of these represents the onset of self-gravitation, and the second reflects the onset of rotational support. Once the star formation efficiency reaches a few percent, the PDF becomes statistically steady, with no evidence for secular time-evolution at star formation efficiencies from about five to 20 percent. We show that both the Mach number and the virial parameter influence the characteristic densities at which the log-normal gives way to the first power-law, and the first to the second, and we extend (for the former) and develop (for the latter) simple theoretical models for the relationship between these density thresholds and the global properties of the turbulent medium.

16. The Transition of Polarized Dust Thermal Emission from the Protostellar Envelope to the Disk Scale

Ka Ho Lam, Che-Yu Chen, Zhi-Yun Li, Haifeng Yang, Erin G. Cox, Leslie W. Looney, Ian Stephens

Polarized dust continuum emission has been observed with ALMA in an increasing number of deeply embedded protostellar systems. It generally shows a sharp transition going from the protostellar envelope to the disk scale, with the polarization fraction typically dropping from $\sim$5% to $\sim$1% and the inferred magnetic field orientations becoming more aligned with the major axis of the system. We quantitatively investigate these observational trends using a sample of protostars in the Perseus molecular cloud and compare these features with a non-ideal MHD disk formation simulation. We find that the gas density increases faster than the magnetic field strength in the transition from the envelope to the disk scale, which makes it more difficult to magnetically align the grains on the disk scale. Specifically, to produce the observed $\sim$1% polarization at $\sim$100 au scale via grains aligned with the B-field, even relatively small grains of 1 μm in size need to have their magnetic susceptibilities significantly enhanced (by a factor of $\sim$20) over the standard value, potentially through superparamagnetic inclusions. This requirement is more stringent for larger grains, with the enhancement factor increasing linearly with the grain size, reaching $\sim 2 \times 10^4$ for millimeter-sized grains. Even if the required enhancement can be achieved, the resulting inferred magnetic field orientation in the simulation does not show a preference for the major axis, which is inconsistent with the observed pattern. We thus conclude that the observed trends are best described by the model where the polarization on the envelope scale is dominated by magnetically aligned grains and that on the disk scale by scattering.

17. The link between gas and stars in the S254-S258 star-forming region

D. A. Ladeyschikov, M. S. Kirsanova, A. M. Sobolev, M. Thomasson, V. Ossenkopf-Okada, M. Juvela, S. A. Khaibrakhmanov, E. A. Popova

The paper aims to study relation between the distributions of the young stellar objects (YSOs) of different ages and the gas-dust constituents of the S254-S258 star-formation complex. This is necessary to study the time evolution of the YSO distribution with respect to the gas and dust compounds which are responsible for the birth of the young stars. For this purpose we use correlation analysis between different gas, dust and YSOs tracers. We compared the large-scale CO, HCO^+, near-IR extinction, and far-IR *Herschel* maps with the density of YSOs of the different evolutionary Classes. The direct correlation analysis between these maps was used together with the wavelet-based spatial correlation analysis. This analysis reveals a much tighter correlation of the gas-dust tracers with the distribution of Class I YSOs than with that of Class II YSOs. We argue that Class I YSOs which were initially born in the central bright cluster S255-IR (both N and S parts) during their evolution to Class II stage ($\sim$2 Myr) had enough time to travel through the whole S254-S258 star-formation region. Given that the region contains several isolated YSO clusters, the evolutionary link between these clusters and the bright central S255-IR (N and S) cluster can be considered. Despite the complexity of the YSO cluster formation in the non-uniform medium, the clusters of Class II YSOs in the S254-258 star-formation region can contain objects born in the different locations of the complex.

18. SiO Outflows as Tracers of Massive Star Formation in Infrared Dark Clouds

Mengyao Liu, Jonathan C. Tan, Joshua Marvil, Shuo Kong, Viviana Rosero, Paola Caselli, Giuliana Cosentino

To study the early phases of massive star formation, we present ALMA observations of SiO(5-4) emission and VLA observations of 6 cm continuum emission towards 32 Infrared Dark Cloud (IRDC) clumps, spatially resolved down to $\lesssim$ 0.05 pc. Out of the 32 clumps, we detect SiO emission in 20 clumps, and in 11 of them the SiO emission is relatively strong and likely tracing protostellar outflows. Some SiO outflows are collimated, while others are less ordered. For the six strongest SiO outflows, we estimate basic outflow properties. In our entire sample, where there is SiO emission, we find 1.3 mm continuum and infrared emission nearby, but not vice versa. We build the spectral energy distributions (SEDs) of cores with 1.3 mm continuum emission

and fit them with radiative transfer (RT) models. The low luminosities and stellar masses returned by SED fitting suggest these are early stage protostars. We see a slight trend of increasing SiO line luminosity with bolometric luminosity, which suggests more powerful shocks in the vicinity of more massive YSOs. We do not see a clear relation between the SiO luminosity and the evolutionary stage indicated by L/M. We conclude that as a protostar approaches a bolometric luminosity of $\sim 10^2\ L_\odot$, the shocks in the outflow are generally strong enough to form SiO emission. The VLA 6 cm observations toward the 15 clumps with the strongest SiO emission detect emission in four clumps, which is likely shock ionized jets associated with the more massive ones of these protostellar cores.

19. Massive Protocluster of a Periodic Maser Source G188.95+0.89

M. M. Mutie, J. O. Chibueze, K. El Bouchefry, G. C. MacLeod, J. Morgan, P. Baki

We report the results of ongoing monitoring of the 6.7 GHz CH_3OH masers associated with G188.95+0.89. In these observations five features are periodically varying and at least two exhibit evidence of velocity drifts. It is not clear the cause of these velocity drifts. The spectra have varied significantly since detection in 1991. The 11.45 km s^1 feature has decreased exponentially from 2003. Complementary ALMA 1.3 mm continuum and line observational results are also presented. Eight continuum cores (MM1 - MM8) were detected in G188.95+0.89. We derived the masses of the detected cores. G188.95+0.89 MM2 was resolved into 2 continuum cores (separated by 0.1 arcsec) in ALMA band 7 observations. Also CH_3OH ($4_{(2,2)}$-$3_{(1,2)}$) thermal emission associated with MM2 is double peaked. We propose the presence of multiple (at least binary) young stellar objects in MM2. SiO emission exhibit a bow-shock morphology in MM2 while strong emission of ^{12}CO at the east and west of MM2 suggest the presence of an east-west bipolar outflow.

20. Proper motions of spectrally selected structures in the HH 83 outflow

T. A. Movsessian, T. Yu. Magakian, A. V. Moiseev

We continue our program of investigation of the proper motions of spectrally separated structures in the Herbig-Haro outflows with the aid of Fabry-Perot scanning interferometry. This work mainly focuses on the physical nature of various structures in the jets. The aim of the present study is to measure the proper motions of the previously discovered kinematically separated structures in the working surface of the HH 83 collimated outflow. We used observations from two epochs separated by 15 years, which were performed on the 6m telescope with Fabry-Perot scanning interferometer. We obtained images corresponding to different radial velocities for the two separate epochs, and used them to measure proper motions. In the course of our data analysis, we discovered a counter bow-shock of HH 83 flow with positive radial velocity, which makes this flow a relatively symmetric bipolar system. The second epoch observations confirm that the working surface of the flow is split into two structures with an exceptionally large (250 km s^{-1}) difference in radial velocity. The proper motions of these structures are almost equal, which suggests that they are physically connected. The asymmetry of the bow shock and the turning of proper motion vectors suggests a collision between the outflow and a dense cloud. The profile of the Hα line for the directly invisible infrared source HH 83 IRS, obtained by integration of the data within the reflection nebula, suggests it to be of P Cyg type with a broad absorption component characteristic of the FU Ori like objects. If this object underwent an FU Ori type outburst, which created the HH 83 working surfaces, its eruption took place about 1500 years ago according to the kinematical age of the outflow.

21. Characterization of dense Planck clumps observed with Herschel and SCUBA-2

E. Mannfors, M. Juvela, L. Bronfman, D. J. Eden, Jinhua He, Gwanjeon Kim, Kee-Tae Kim, H. Kirppu, T. Liu, J. Montillaud, H. Parsons, Patricio Sanhueza, Hsien Shang, A. Soam, K. Tatematsu, A. Traficante, M. S. Väisälä, Chang Won Lee

We aim to characterize a diverse selection of dense, potentially star-forming cores, clumps, and clouds within the Milky Way in terms of their dust emission and SF activity. We studied 53 fields that have been observed in the JCMT SCUBA-2 continuum survey SCOPE and have been mapped with Herschel. We estimated dust properties by fitting Herschel observations with modified blackbody functions, studied the relationship between dust temperature and dust opacity spectral index β, and estimated column densities. We extracted clumps from the SCUBA-2 850 μm maps with the FellWalker algorithm and examined their masses and sizes. Clumps are associated with young stellar objects found in several catalogs. We estimated the gravitational stability of the clumps with virial analysis. The clumps are categorized as unbound starless, prestellar, or protostellar. We find 529 dense clumps, typically with high column densities from (0.3-4.8)$\times 10^{22}$ cm^{-2}, with a mean of (1.5$\pm$0.04)$\times 10^{22}$ cm^{-2}, low temperatures (T $\sim$10-20 K), and estimated submillimeter β =1.7$\pm$0.1. We detect a slight increase in opacity spectral index toward millimeter wavelengths. Masses of the sources range from 0.04 $M_\odot$ to 4259 $M_\odot$. Mass, linear size, and temperature are correlated with distance. Furthermore, the estimated gravitational stability is dependent on distance, and more distant clumps appear more virially bound. Finally, we present a catalog of properties of the clumps.Our sources present a large array of SF

regions, from high-latitude, nearby diffuse clouds to large SF complexes near the Galactic center. Analysis of these regions will continue with the addition of molecular line data, which will allow us to study the densest regions of the clumps in more detail.

22. A major asymmetric ice trap in a planet-forming disk: I. Formaldehyde and methanol

N. van der Marel, A. S. Booth, M. Leemker, E. F. van Dishoeck, S. Ohashi

The chemistry of planet-forming disks sets the exoplanet atmosphere composition and the prebiotic molecular content. Dust traps are of particular importance as pebble growth and transport are crucial for setting the chemistry where giant planets are forming. The asymmetric Oph IRS 48 dust trap located at 60 au radius provides a unique laboratory for studying chemistry in pebble-concentrated environments in warm Herbig disks with low gas-to-dust ratios down to 0.01. We use deep ALMA Band 7 line observations to search the IRS 48 disk for H_2CO and CH_3OH line emission, the first steps of complex organic chemistry. We report the detection of 7 H_2CO and 6 CH_3OH lines with energy levels between 17 and 260 K. The line emission shows a crescent morphology, similar to the dust continuum, suggesting that the icy pebbles play an important role in the delivery of these molecules. Rotational diagrams and line ratios indicate that both molecules originate from warm molecular regions in the disk with temperatures >100 K and column densities $\sim 10^{14}$ cm^{-2} or a fractional abundance of $\sim 10^{-8}$ and with $H_2CO/CH_3OH \sim 0.2$, indicative of ice chemistry. Based on arguments from a physical-chemical model with low gas-to-dust ratios, we propose a scenario where the dust trap provides a huge icy grain reservoir in the disk midplane or an 'ice trap', which can result in high gas-phase abundances of warm COMs through efficient vertical mixing. This is the first time that complex organic molecules have been clearly linked to the presence of a dust trap. These results demonstrate the importance of including dust evolution and vertical transport in chemical disk models, as icy dust concentrations provide important reservoirs for complex organic chemistry in disks.

23. A stellar mass dependence of structured disks: a possible link with exoplanet demographics

Nienke van der Marel, Gijs Mulders

Gaps in protoplanetary disks have long been hailed as signposts of planet formation. However, a direct link between exoplanets and disks remains hard to identify. We present a large sample study of ALMA disk surveys of nearby star-forming regions to disentangle this connection. All disks are classified as either structured (transition, ring, extended) or non-structured (compact) disks. Although low-resolution observations may not identify large scale substructure, we assume that an extended disk must contain substructure from a dust evolution argument. A comparison across ages reveals that structured disks retain high dust masses up to at least 10 Myr, whereas the dust mass of compact, non-structured disks decreases over time. This can be understood if the dust mass evolves primarily by radial drift, unless drift is prevented by pressure bumps. We identify a stellar mass dependence of the fraction of structured disks. We propose a scenario linking this dependence with that of giant exoplanet occurrence rates. We show that there are enough exoplanets to account for the observed disk structures if transitional disks are created by exoplanets more massive than Jupiter, and ring disks by exoplanets more massive than Neptune, under the assumption that most of those planets eventually migrate inwards. On the other hand, the known anti-correlation between transiting super-Earths and stellar mass implies those planets must form in the disks without observed structure, consistent with formation through pebble accretion in drift-dominated disks. These findings support an evolutionary scenario where the early formation of giant planets determines the disk's dust evolution and its observational appearance.

24. Spectral index of synchrotron emission: insights from the diffuse and magnetised interstellar medium

Marco Padovani, Andrea Bracco, Vibor Jelić, Daniele Galli, Elena Bellomi

The interpretation of Galactic synchrotron observations is complicated by the degeneracy between the strength of the magnetic field perpendicular to the line of sight (LOS), $B_\perp$, and the cosmic-ray electron (CRe) spectrum. Depending on the observing frequency, an energy-independent spectral energy slope s for the CRe spectrum is usually assumed: $s = -2$ at frequencies below $\simeq$400 MHz and $s = -3$ at higher frequencies. Motivated by the high angular and spectral resolution of current facilities such as the LOw Frequency ARray (LOFAR) and future telescopes such as the Square Kilometre Array (SKA), we aim to understand the consequences of taking into account the energy-dependent CRe spectral energy slope on the analysis of the spatial variations of the brightness temperature spectral index, β, and on the estimate of the average value of $B_\perp$ along the LOS. We illustrate analytically and numerically the impact that different realisations of the CRe spectrum have on the interpretation of the spatial variation of β. We find that the common assumption of an energy-independent s is valid only in special cases. We show that for typical magnetic field strengths of the diffuse interstellar medium ($\simeq 2-20$ μG), at frequencies of 0.1$-$10 GHz, the electrons that are mainly responsible for the synchrotron emission have energies in the range $\simeq$100 MeV$-$50 GeV. This is the energy

range where the spectral slope, s, of CRe has its greatest variation. We also show that the polarisation fraction can be much smaller than the maximum value of $\simeq 70\%$ because the orientation of $\mathbf{B}_\perp$ varies across the telescope's beam and along the LOS. Finally, we present a look-up plot that can be used to estimate the average value of $B_\perp$ along the LOS from a set of values of β measured at centimetre to metre wavelengths, for a given CRe spectrum.

25. Molecular line signatures of cloud-cloud collisions

F. D. Priestley, A. P. Whitworth

Collisions between interstellar gas clouds are potentially an important mechanism for triggering star formation. This is because they are able to rapidly generate large masses of dense gas. Observationally, cloud collisions are often identified in position-velocity (PV) space through bridging features between intensity peaks, usually of CO emission. Using a combination of hydrodynamical simulations, time-dependent chemistry, and radiative transfer, we produce synthetic molecular line observations of overlapping clouds that are genuinely colliding, and overlapping clouds that are just chance superpositions. Molecules tracing denser material than CO, such as NH_3 and HCN, reach peak intensity ratios of 0.5 and 0.2 with respect to CO in the 'bridging feature' region of PV space for genuinely colliding clouds. For overlapping clouds that are just chance superpositions, the peak NH_3 and HCN intensities are co-located with the CO intensity peaks. This represents a way of confirming cloud collisions observationally, and distinguishing them from chance alignments of unrelated material.

26. Understanding the angular momentum evolution of T Tauri and Herbig Ae/Be stars

Giovanni Pinzón, Jesús Hernández, Javier Serna, Alexandra García, Ezequiel Manzo-Martínez, Alexandre Roman-Lopes, Carlos G. Román-Zúñiga, Maria Gracia Batista, Julio Ramírez-Vélez, Yeisson Osorio, Ronald Avendaño

We investigate a sample of 6 Herbig Ae/Be stars belonging to the Orion OB1 association, as well as 73 low mass objects, members of the σ Orionis cluster, in order to explore the angular momentum evolution at early stages of evolution, and its possible connection with main-sequence Ap/Bp magnetic stars. Using FIES and HECTOCHELLE spectra, we obtain projected rotational velocities through two independent methods. Individual masses, radii, and ages were computed using evolutionary models, distance, and cluster extinction. Under the assumption that similar physical processes operate in both, T Tauri and Herbig Ae/Be stars, we construct snapshots of the protostar's rotation against mass during the first 10 Myr with the aid of a rotational model that includes a variable disc lifetime, changes in the stellar moment of inertia, a dipolar magnetic field with variable strength, and angular momentum loss through stellar winds powered by accretion. We use these snapshots, as well as the rotational data, to infer a plausible scenario for the angular momentum evolution. We find that magnetic field strengths of a few kG at 3 Myr are required to match the rotational velocities of both groups of stars. Models with masses between 2-3 $M_\odot$ display larger angular momentum by a factor of ~ 3, in comparison to stars of similar spectral types on the main-sequence. Even though some quantitative estimates on this dramatic decrease with age, for Ap/Bp magnetic main-sequence stars are presented, the results obtained for the angular momentum evolution do not explain their low rotation.

27. Self-Sustaining Vortices in Protoplanetary Disks: Setting the Stage for Planetary System Formation

Zsolt Regaly, Kundan Kadam, Cornelis P. Dullemond

The core accretion scenario of planet formation assumes that planetesimals and planetary embryos are formed during the primordial, gaseous phases of the protoplanetary disk. However, how the dust particles overcome the traditional growth barriers is not well understood. The recently proposed viscous ring-instability may explain the concentric rings observed in protoplanetary disks by assuming that the dust grains can reduce the gas conductivity, which can weaken the magneto-rotational instability. We present an analysis of this model with the help of GPU-based numerical hydrodynamic simulations of coupled gas and dust in the thin-disk limit. During the evolution of the disk the dusty rings become Rossby unstable and break up into a cascade of small-scale vortices. The vortices form secularly stable dusty structures, which could be sites of planetesimal formation by the streaming instability as well as direct gravitational collapse. The phenomenon of self-sustaining vortices is consistent with observational constraints of exoplanets and sets a favorable environment for planetary system formation.

28. Physical conditions in the warped accretion disk of a massive star. 349 GHz ALMA observations of G023.01−00.41

A. Sanna, A. Giannetti, M. Bonfand, L. Moscadelli, R. Kuiper, J. Brand, R. Cesaroni, A. Caratti o Garatti, T. Pillai, K. M. Menten

Young massive stars warm up the large amount of gas and dust which condenses in their vicinity, exciting a forest of lines from different molecular species. Their line brightness is a diagnostic tool of the gas physical conditions locally, which we use to set constraints on the environment where massive stars form. We made use of the Atacama Large Millimeter/submillimeter Array at frequencies near 349 GHz, with an angular resolution of 0.1″, to observe the methyl cyanide (CH_3CN) emission which arises from the accretion disk of a young massive star. We sample the disk midplane with twelve distinct beams, where we get an independent measure of the gas (and dust) physical conditions. The accretion disk extends above the midplane showing a double-armed spiral morphology projected onto the plane of the sky, which we sample with ten additional beams: along these apparent spiral features, gas undergoes velocity gradients of about 1kms^{-1} per 2000 au. The gas temperature (T) rises symmetrically along each side of the disk, from about 98 K at 3000 au to 289 K at 250 au, following a power law with radius, $R^{-0.43}$. The CH_3CN column density (N) increases from 9.2×10^{15}cm^{-2} to 8.7×10^{17}cm^{-2} at the same radii, following a power law with radius, $R^{-1.8}$. In the framework of a circular gaseous disk observed approximately edge-on, we infer an H_2 volume density in excess of 4.8×10^9cm^{-3} at a distance of 250 au from the star. We study the disk stability against fragmentation following the methodology by Kratter et al. (2010), appropriate under rapid accretion, and we show that the disk is marginally prone to fragmentation along its whole extent.

29. FORCAST imaging of two small nearby Clusters: The Coronet and B59

G. Sandell, B. Reipurth, W. D. Vacca, N. S. Bajaj

We present mid infrared imaging of two young clusters, the Coronet in the CrA cloud core and B59 in the Pipe Nebula, using the FORCAST camera on the Stratospheric Observatory for Infrared Astronomy. We also analyze Herschel Space Observatory PACS and SPIRE images of the associated clouds. The two clusters are at similar, and very close, distances. Star formation is ongoing in the Coronet, which hosts at least one Class 0 source and several pre-stellar cores, which may collapse and form stars. The B59 cluster is older, although it still has a few Class I sources, and is less compact. The CrA cloud has a diameter of about 0.16 pc, and we determine a dust temperature of 15.7 K and a star formation efficiency of about 27 twice as large, has a dust temperature of about 11.4 K and a star formation efficiency of about 14 the Coronet, which has also formed intermediate mass stars, while B59 has only formed low-mass stars.

30. Chandra X-ray Observations of V830 Tau: A T Tauri Star Hosting an Evanescent Planet

Stephen L. Skinner, Manuel Guedel

A radial velocity study by Donati et al. (2016) reported the detection of a close-in giant planet in a 4.93 d orbit around the 2 Myr old weak-lined T Tauri star V830 Tau. Because of the stringent timescale constraints that a very young host star like V830 Tau would place on hot Jupiter formation models and inward migration mechanisms, independent confirmation of the planet's existence is needed but so far has not been obtained. We present new Chandra X-ray observations of V830 Tau. The Chandra observations in combination with previous XMM-Newton observations reveal strong variable X-ray emission with an X-ray luminosity spanning the range log Lx = 30.10 - 30.87 ergs/s. Chandra High Energy Transmission Grating (HETG) spectra show emission lines formed over a range of plasma temperatures from 4 MK (Ne IX) to 16 MK (S XV). At the separation of the reported planet (0.057 au) the X-ray flux is 10^6 - 10^7 times greater than the Sun's X-ray flux at Jupiter. We provide estimates of the X-ray ionization and atmospheric heating rates at the planet's separation and identify areas of uncertainty that will need to be addressed in any future atmospheric models.

31. X-raying the Sco-Cen OB association: The low-mass stellar population revealed by eROSITA

J. H. M. M. Schmitt, S. Czesla, S. Freund, J. Robrade, P. C. Schneider

We present the results of the first X-ray all-sky survey (eRASS1) performed by the eROSITA instrument on board the Spectrum-Roentgen-Gamma (SRG) observatory of the Sco-Cen OB association. Bona fide Sco-Cen member stars are young and are therefore expected to emit X-rays at the saturation level. The sensitivity limit of eRASS1 makes these stars detectable down to about a tenth of a solar mass. By cross-correlating the eRASS1 source catalog with the Gaia EDR3 catalog, we arrive at a complete identification of the stellar (i.e., coronal) source content of eROSITA in the Sco-Cen association, and in particular obtain for the first time a 3D view of the detected stellar X-ray sources. Focusing on the low-mass population and placing the

optical counterparts identified in this way in a color-magnitude diagram, we can isolate the young stars out of the detected X-ray sources and obtain age estimates of the various Sco-Cen populations. A joint analysis of the 2D and 3D space motions, the latter being available only for a smaller subset of the detected stellar X-ray sources, reveals that the space motions of the selected population show a high degree of parallelism, but there is also an additional population of young, X-ray emitting and essentially cospatial stars that appears to be more diffuse in velocity space. Its nature is currently unclear. We argue that with our procedures, an identification of almost the whole stellar content of the Sco-Cen association will become possible once the final Gaia and eROSITA catalogs are available by the end of this decade. We furthermore call into question any source population classification scheme that relies on purely kinematic selection criteria.

32. The filamentary structures in the CO emission toward the Milky Way disk

J. D. Soler, H. Beuther, J. Syed, Y. Wang, Th. Henning, S. C. O. Glover, R. S. Klessen, M. C. Sormani, M. Heyer, R. J. Smith, J. S. Urquhart, J. Yang, Y. Su, X. Zhou

We present a statistical study of the filamentary structure orientation in the CO emission observations obtained in the Milky Way Imaging Scroll Painting (MWISP) survey in the range $25.8\,\mathrm{deg} < l < 49.7\,\mathrm{deg}$, $|b| \leq 1.25\,\mathrm{deg}$, and $-100 < v_{\mathrm{LSR}} < 135$ km/s. We found that most of the filamentary structures in the ^{12}CO and ^{13}CO emission do not show a global preferential orientation either parallel or perpendicular to the Galactic plane. However, we found ranges in Galactic longitude and radial velocity where the ^{12}CO and ^{13}CO filamentary structures are parallel to the Galactic plane. These preferential orientations are different from those found for the HI emission. We consider this an indication that the molecular structures do not simply inherit these properties from parental atomic clouds. Instead, they are shaped by local physical conditions, such as stellar feedback, magnetic fields, and Galactic spiral shocks.

33. The general applicability of self-similar solutions for thermal disc winds

Andrew D. Sellek, Cathie J. Clarke, Richard A. Booth

Thermal disc winds occur in many contexts and may be particularly important to the secular evolution and dispersal of protoplanetary discs heated by high energy radiation from their central star. In this paper we generalise previous models of self-similar thermal winds - which have self-consistent morphology and variation of flow variables - to the case of launch from an elevated base and to non-isothermal conditions. These solutions are well-reproduced by hydrodynamic simulations, in which, as in the case of isothermal winds launched from the mid-plane, we find winds launch at the maximum Mach number for which the streamline solutions extend to infinity without encountering a singularity. We explain this behaviour based on the fact that lower Mach number solutions do not fill the spatial domain. We also show that hydrodynamic simulations reflect the corresponding self-similar models across a range of conditions appropriate to photoevaporating protoplanetary discs, even when gravity, centrifugal forces, or changes in the density gradient mean the problem is not inherently scale free. Of all the parameters varied, the elevation of the wind base affected the launch velocity and flow morphology most strongly, with temperature gradients causing only minor differences. We explore how launching from an elevated base affects Ne II line profiles from winds, finding it increases (reduces) the full width at half maximum (FWHM) of the line at low (high) inclination to the line of sight compared with models launched from the disc mid-plane and thus weakens the dependence of the FWHM on inclination.

34. Long-term optical photometric monitoring of the FUor star V900 Mon

Evgeni Semkov, Stoyanka Peneva, Sunay Ibryamov

We present results from photometric monitoring of V900 Mon, one of the newly discovered and still under-studied object from FU Orionis type. FUor phenomenon is very rarely observed, but it is essential for stellar evolution. Since we only know about twenty stars of this type, the study of each new object is very important for our knowledge. Our data was obtained in the optical spectral region with BVRI Johnson-Cousins set of filters during the period from September 2011 to April 2021. In order to follow the photometric history of the object, we measured its stellar magnitudes on the available plates from the Mikulski Archive for Space Telescopes. The collected archival data suggests that the rise in brightness of V900 Mon began after January 1989 and the outburst goes so far. In November 2009, when the outburst was registered, the star had already reached a level of brightness close to the current one. Our observations indicate that during the period 2011-2017 the stellar magnitude increased gradually in each pass band. The observed amplitude of the outburst is about 4 magnitudes (R). During the last three years, the increase in brightness has stopped and there has even been a slight decline. The comparison of the light curves of the known FUor objects shows that they are very diverse and are rarely repeated. However, the photometric data we have so far shows that the V900 Mon's light curve is somewhat similar to this of V1515 Cyg and V733 Cep.

35. Which molecule traces what: chemical diagnostics of protostellar sources

Łukasz Tychoniec, Ewine F. van Dishoeck, Merel L. R. van 't Hoff, Martijn L. van Gelder, Benoît Tabone, Yuan Chen, Daniel Harsono, Charles L. H. Hull, Michiel R. Hogerheijde, Nadia M. Murillo, John J. Tobin

The physical and chemical conditions in Class 0/I protostars are fundamental in unlocking the protostellar accretion process and its impact on planet formation. The aim is to determine which physical components are traced by different molecules at sub-arcsecond scales (100 - 400 au). We use a suite of Atacama Large Millimeter/submillimeter Array (ALMA) datasets in Band 6 (1 mm), Band 5 (1.8 mm) and Band 3 (3 mm) at spatial resolutions 0.5 - 3" for 16 protostellar sources. The protostellar envelope is well traced by $C^{18}O$, DCO^+ and N_2D^+, with the freeze-out of CO governing the chemistry at envelope scales. Molecular outflows are seen in classical shock tracers like SiO and SO, but ice-mantle products such as CH_3OH and HNCO released with the shock are also observed. The molecular jet is prominent not only in SiO and SO but also occasionally in H_2CO. The cavity walls show tracers of UV-irradiation such as C_2H c-C_3H_2 and CN. The hot inner envelope, apart from showing emission from complex organic molecules (COMs), also presents compact emission from small molecules like H_2S, SO, OCS and $H^{13}CN$, most likely related to ice sublimation and high-temperature chemistry. Sub-arcsecond millimeter-wave observations allow to identify those (simple) molecules that best trace each of the physical components of a protostellar system. COMs are found both in the hot inner envelope (high excitation lines) and in the outflows (lower-excitation lines) with comparable abundances. COMs can coexist with hydrocarbons in the same protostellar sources, but they trace different components. In the near future, mid-IR observations with JWST-MIRI will provide complementary information about the hottest gas and the ice mantle content, at unprecedented sensitivity and at resolutions comparable to ALMA for the same sources.

36. Probing protoplanetary disk evolution in the Chamaeleon II region

M. Villenave, F. Menard, W. R. F. Dent, M. Benisty, G. van der Plas, J. P. Williams, M. Ansdell, A. Ribas, C. Caceres, H. Canovas, L. Cieza, A. Hales, I. Kamp, C. Pinte, D. A. Principe, M. R. Schreiber

Context. Characterizing the evolution of protoplanetary disks is necessary to improve our understanding of planet formation. Constraints on both dust and gas are needed to determine the dominant disk dissipation mechanisms. Aims. We aim to compare the disk dust masses in the Chamaeleon II (Cha II) star-forming region with other regions with ages between 1 and 10Myr. Methods. We use ALMA band 6 observations (1.3 mm) to survey 29 protoplanetary disks in Cha II. Dust mass estimates are derived from the continuum data. Results. Out of our initial sample of 29 disks, we detect 22 sources in the continuum, 10 in 12CO, 3 in 13CO, and none in C18O (J=2-1). Additionally, we detect two companion candidates in the continuum and 12CO emission. Most disk dust masses are lower than 10Mearth, assuming thermal emission from optically thin dust. We compare consistent estimations of the distributions of the disk dust mass and the disk-to-stellar mass ratios in Cha II with six other low mass and isolated star-forming regions in the age range of 1-10Myr: Upper Sco, CrA, IC 348, Cha I, Lupus, and Taurus. When comparing the dust-to-stellar mass ratio, we find that the masses of disks in Cha II are statistically different from those in Upper Sco and Taurus, and we confirm that disks in Upper Sco, the oldest region of the sample, are statistically less massive than in all other regions. Performing a second statistical test of the dust mass distributions from similar mass bins, we find no statistical differences between these regions and Cha II. Conclusions. We interpret these trends, most simply, as a sign of decline in the disk dust masses with time or dust evolution. Different global initial conditions in star-forming regions may also play a role, but their impact on the properties of a disk population is difficult to isolate in star-forming regions lacking nearby massive stars.

37. From downtown to the outskirts: a radio survey of the Orion Nebula Cluster

Jaime Vargas-González, Jan Forbrich, Sergio A. Dzib, John Bally

We present a newly enlarged census of the compact radio population towards the Orion Nebula Cluster (ONC) using high-sensitivity continuum maps (3-10 μJy bm^{-1}) from a total of $\sim$ 30 h centimeter-wavelength observations over an area of $\sim 20' \times 20'$ obtained in the C-band (4−8 GHz) with the Karl G. Jansky Very Large Array (VLA) in its high-resolution A-configuration. We thus complement our previous deep survey of the innermost areas of the ONC, now covering the field of view of the Chandra Orion Ultra-deep Project (COUP). Our catalog contains 521 compact radio sources of which 198 are new detections. Overall, we find that 17COUP sources have radio counterparts, while 53counterparts. Most notably, the radio detection fraction of X-ray sources is higher in the inner cluster and almost constant for $r > 3'$ (0.36 pc) from θ^1 Ori C suggesting a correlation between the radio emission mechanism of these sources and their distance from the most massive stars at the center of the cluster, for example due to increased photoionisation of circumstellar disks. The combination with our previous observations four years prior lead to the discovery of fast proper motions of up to $\sim$373 km s^{-1} from faint radio sources associated with ejecta of the OMC1 explosion. Finally, we search for strong radio variability. We found changes in flux density by a factor of $\lesssim$5 within our observations and a few sources with changes by a factor >10 on long timescales of a few years.

38. Evidence of Accretion Burst: The Viscously Heated Inner Disk of the Embedded Protostar IRAS 16316-1540

Sung-Yong Yoon, Jeong-Eun Lee, Seokho Lee, Gregory J. Herczeg, Sunkyung Park, Gregory N. Mace, Jae-Joon Lee, Daniel T. Jaffe

Outbursts of young stellar objects occur when the mass accretion rate suddenly increases. However, such outbursts are difficult to detect for deeply embedded protostars due to their thick envelope and the rarity of outbursts. The near-IR spectroscopy is a useful tool to identify ongoing outburst candidates by the characteristic absorption features that indicate a disk origin. However, without high-resolution spectroscopy, the spectra of outburst candidates can be confused with the late-type stars since they have similar spectral features. For the protostar IRAS 16316-1540, the near-IR spectrum has line equivalent widths that are consistent with M-dwarf photospheres. However, our high-resolution IGRINS spectra reveal that the absorption lines have boxy and/or double-peaked profiles, as expected from a disk and not the star. The continuum emission source is likely the hot, optically thick disk, heated by viscous accretion. The projected disk rotation velocity of 41 ± 5 km s^{-1} corresponds to ~ 0.1 AU. Based on the result, we suggest IRAS 16316-1540 as an ongoing outburst candidate. Viscous heating of disks is usually interpreted as evidence for ongoing bursts, which may be more common than previously estimated from low-resolution near-IR spectra.

39. ALMA discovery of a dual dense probably rotating outflow from a massive young stellar object G18.88MME

I. I. Zinchenko, L. K. Dewangan, T. Baug, D. K. Ojha, N. K. Bhadari

We report the discovery of a very dense jet-like fast molecular outflow surrounded by a wide-angle wind in a massive young stellar object (MYSO) G18.88MME (stellar mass $\sim$8 $M_\odot$) powering an Extended Green Object G18.89−0.47. Four cores MM1-4 are identified in the Atacama Large Millimeter/submillimeter Array (ALMA) 1.3 mm continuum map (resolution $\sim$0."8) toward G18.88MME, and are seen at the center of the emission structure (extent $\sim$0.3 pc $\times$ 0.2 pc) detected in the ALMA map. G18.88MME is embedded in the core MM1 (mass $\sim$13-18 $M_\odot$), where no radio continuum emission is detected. The molecular outflow centered at MM1 is investigated in the SiO(5-4), HC_3N(24-23) and ^{13}CO(2-1) lines. The detection of HC_3N in the outflow is rare in MYSOs and indicates its very high density. The position-velocity diagrams display a fast narrow outflow (extent $\sim$28000 AU) and a slower wide-angle more extended outflow toward MM1, and both of these components show a transverse velocity gradient indicative of a possible rotation. All these observed features together make G18.88MME as a unique object for studying the unification of the jet-driven and wind-driven scenarios of molecular outflows in MYSOs.